

Quantifying Photon Recycling in Solar Cells and Light-Emitting Diodes: Absorption and Emission Are Always Key

Alan R. Bowman¹, Miguel Anaya¹, Neil C. Greenham¹, and Samuel D. Stranks^{1,2,*}

¹*Cavendish Laboratory, Department of Physics, University of Cambridge, J.J. Thomson Avenue, Cambridge CB3 0HE, United Kingdom*

²*Department of Chemical Engineering & Biotechnology, University of Cambridge, Philippa Fawcett Drive, Cambridge CB3 0AS, United Kingdom*

 (Received 17 January 2020; revised 9 April 2020; accepted 24 June 2020; published 5 August 2020)

Photon recycling has received increased attention in recent years following its observation in halide perovskites. It has been shown to lower the effective bimolecular recombination rate and thus increase excitation densities within a material. Here we introduce a general framework to quantify photon recycling which can be applied to any material. We apply our model to idealized solar cells and light-emitting diodes based on halide perovskites. By varying controllable parameters which affect photon recycling, namely, thickness, charge trapping rate, nonideal transmission at interfaces, and absorptance, we quantify the effect of each on photon recycling. In both device types, we demonstrate that maximizing absorption and emission processes remains paramount for optimizing devices, even if this is at the expense of photon recycling. Our results provide new insight into quantifying photon recycling in optoelectronic devices and demonstrate that photon recycling cannot always be seen as a beneficial process.

DOI: [10.1103/PhysRevLett.125.067401](https://doi.org/10.1103/PhysRevLett.125.067401)

Photon recycling has been reported in luminescent semiconductors including GaAs, InP, and, more recently, halide perovskites such as methylammonium lead iodide (MAPbI₃) [1–4]. It is a direct consequence of the reciprocity between absorption and emission—if a material can emit a photon at a wavelength it can also absorb a photon at that wavelength [5,6]. The role of photon recycling in decreasing radiative recombination rates in perovskites has been discussed [7,8]. Recently, Brenes *et al.* explored the effect of photon recycling on the maximum power point voltage in idealized perovskite solar cells with variable charge trapping rates [9] and demonstrated an increase in maximum power point voltage of 77 mV can be attributed to photon recycling. Similarly, Cho *et al.* recently showed photon recycling to be of importance in perovskite light-emitting diodes [4].

Here, we construct a generalized framework to quantify photon recycling. We make no assumptions about the nature of the excitation, the emission, or the competing loss processes. We calculate the number of photon recycling events per initial excitation, N (from external photon absorption or charge injection), under different device-relevant conditions, allowing us to draw conclusions as to when the phenomenon is most beneficial. We apply our model to idealized MAPbI₃ solar cells and CsPbBr₃ LEDs at operating voltages, and quantify the effect of different controllable parameters. For solar cells, we go beyond previous reports [9] by considering changes in both current and voltage, and their relation to controllable parameters. In both device types, increasing thickness, improving

reflection at the rear interface, and decreasing charge trapping all enhance device performance and N . However, we demonstrate that enhancements due to photon recycling do not compensate for reduced light absorption or emission when considering transmission at the front interface and surface roughness. We conclude that to maximize solar cell or LED performance one must maximize absorptance or emittance, even if this is at the expense of photon recycling.

We begin by introducing the probability an emitted photon of energy E escapes a material, $\eta_{\text{esc}}(E)$, which is given by

$$\eta_{\text{esc}}(E) = \frac{a(E)}{4n(E)^2\alpha(E)t}. \quad (1)$$

Here $n(E)$ is the (real part of the) refractive index, $\alpha(E)$ the absorption coefficient, and t the thickness. To derive this we assume negligible Stokes shift (corresponding to maximized photon recycling), so the absorptance $a(E)$ is equal to the emissivity [5] (see derivation in Supplemental Material [10], Note 2). Subsequent conclusions do not rely on this assumption. Equation (1) demonstrates that maximizing absorptance also maximizes $\eta_{\text{esc}}(E)$ and therefore can reduce N .

As the number of photons emitted at energy E (per unit volume, per unit energy, per unit time) is $4\pi n(E)^2\alpha(E)\Phi_{\text{bb}}(E)e^{(\mu/k_B T)}$ [11], the energy-averaged escape probability is expressed by

$$\begin{aligned}\bar{\eta}_{\text{esc}} &= \frac{\int (\text{No. of photons emitted at } E) \times \eta_{\text{esc}}(E) dE}{\int (\text{No. of photons emitted at } E) dE} \\ &= \frac{\int \pi \alpha(E) \Phi_{bb}(E) dE}{t \int 4\pi n(E)^2 \alpha(E) \Phi_{bb}(E) dE},\end{aligned}\quad (2)$$

in agreement with derivations from thermodynamic considerations [6]. Here $\Phi_{bb}(E)$ is the photon flux emitted by the surface of a black body into air (per unit area, per unit solid angle, per unit energy), μ the quasi Fermi-level splitting, and $k_B T$ the thermal energy.

All excitations undergo either radiative or nonradiative decay, with (internal) rates R_r and R_{nr} . We define internal photoluminescence quantum efficiency, PLQE_{int} (or, for electrical injection, internal electroluminescence quantum efficiency), as the ratio of radiative recombination to total recombination,

$$\text{PLQE}_{\text{int}} = \frac{R_r}{R_r + R_{nr}}. \quad (3)$$

The probability of a photon reabsorption event occurring is

$$p = \text{PLQE}_{\text{int}}(1 - \bar{\eta}_{\text{esc}}). \quad (4)$$

A directly measurable quantity is the external PLQE (PLQE_{ext}), the ratio of escaping photons to absorbed incident external excitation [12]. Under steady state illumination, the decay of excitations is balanced by local generation: $G = R_r + R_{nr}$. However, generation is from both incident and recycled photons, thus $G = G_{\text{ext}} + (1 - \bar{\eta}_{\text{esc}})R_r$. Assuming uniform illumination and uniform excitation density,

$$\begin{aligned}\text{PLQE}_{\text{ext}} &= \frac{\text{No. of escaping photons}}{G_{\text{ext}}} = \frac{\bar{\eta}_{\text{esc}} R_r}{\bar{\eta}_{\text{esc}} R_r + R_{nr}} \\ &= \frac{\bar{\eta}_{\text{esc}} \text{PLQE}_{\text{int}}}{1 - (1 - \bar{\eta}_{\text{esc}}) \text{PLQE}_{\text{int}}}.\end{aligned}\quad (5)$$

For a process with probabilities p_i and outcomes X_i , the weighted average is $\sum_i p_i X_i$. Therefore, the average number of photon recycling events per initial excitation is

$$N = \sum_{i=0}^{\infty} i p^i (1-p) = \frac{p}{(1-p)} = \text{PLQE}_{\text{ext}} \left(\frac{1}{\bar{\eta}_{\text{esc}}} - 1 \right). \quad (6)$$

We plot N as a function of PLQE_{ext} and $\bar{\eta}_{\text{esc}}$ in Fig. 1, where the dashed line indicates $N = 1$. This plot is applicable to any material and allows one to assess whether photon recycling is a dominant process (noting PLQE_{ext} and $\bar{\eta}_{\text{esc}}$ should be measured or calculated for the specific material). For $N = 1$ we require $\bar{\eta}_{\text{esc}} < 50\%$ and high PLQE_{ext} , while for materials with large Stokes shift, such as many organic semiconductors, $\bar{\eta}_{\text{esc}} \rightarrow 100\%$, thus there

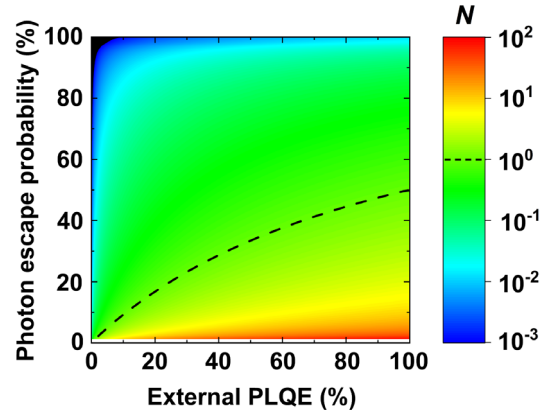


FIG. 1. The number of photon recycling events per initial excitation (N) as a function of the external PLQE (PLQE_{ext}) and the energy-averaged escape probability ($\bar{\eta}_{\text{esc}}$). Dashed line marks one photon recycling event per initial excitation.

is very little photon recycling [note Eqs. (1) and (2) will need modification in case of large Stokes shift].

We now quantify photon recycling in solar cells and LEDs. For solar cells, we use MAPbI_3 from the recently emerged class of halide perovskites. MAPbI_3 has small Stokes shift [13], allowing for computation of $\bar{\eta}_{\text{esc}}$ from Eq. (2). Following the approach of Pazos-Out3n *et al.* [14] we consider MAPbI_3 an intrinsic semiconductor under AM1.5 with recombination due to charge trapping, radiative, and Auger processes (see Supplemental Material [10], Note 3). Unless otherwise stated, our solar cell interacts with radiation from a 2π hemisphere, has a perfect back reflector and no parasitic absorption. We explore four controllable parameters which affect photon recycling: thickness; charge trapping; front and back transmission coefficients; and absorptance (depending on light trapping). While these parameters may be interrelated in any actual solar cell, decoupling these phenomena allows us to quantify their effects on photon recycling. For thickness, trapping rate, and transmission coefficients we use a Beer-Lambert absorptance model (termed direct), though we show similar results from other models in Figs. S1–S11 in the Supplemental Material [10].

We plot the number of photon recycling events at the maximum power point, N_{mpp} , as a function of thickness with no charge trapping in Fig. 2(a). We carried out simulations up to film thicknesses of 1000-nm because charge diffusion lengths are likely to become limiting at larger thicknesses [13]. Even in this idealized case of no trapping, $N_{\text{mpp}} < 1$, primarily because the majority of charges are extracted to the external circuit before they can recombine; at open circuit there can be over 10 photon recycling events [Fig. 2(a), inset]. As thickness increases efficiency and N_{mpp} increase (Figs. S3 and S4 [10]). Efficiency rises due to an increase in short-circuit current (Fig. S5a [10]), while N_{mpp} increases because $\bar{\eta}_{\text{esc}}$ decreases

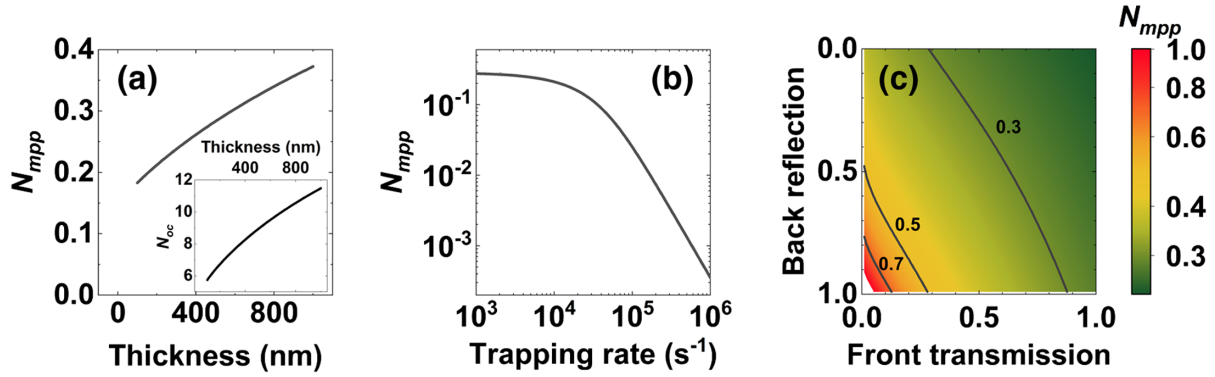


FIG. 2. Number of photon recycling events per absorbed incident photon at maximum power point (N_{mpp}) as a function of (a) thickness (with no charge trapping) and (b) charge trapping for a MAPbI₃ solar cell. Inset in (a) shows the number of photon recycling events at open-circuit voltage (N_{oc}) for the same system as in (a). (c) N_{mpp} on a logarithmic scale with nonideal front transmission and back reflection (no charge trapping). Calculations (b) and (c) are performed on a 500-nm thick film.

significantly (Fig. S6 [10]), while $PLQE_{ext}$ is relatively flat (Fig. S7 [10]).

We show N_{mpp} for a 500-nm thick absorber layer in Fig. 2(b). N_{mpp} falls rapidly from values in Fig. 2(a) unless charge trapping rates are $<10^4 s^{-1}$ (current state of the art is $1 \times 10^5 s^{-1}$, where $N_{mpp} \sim 0.025$ [15]). As charge trapping is decreased, open-circuit voltage increases (Fig. S5b [10]), corresponding to gains in efficiency and N_{mpp} due to reduced nonradiative recombination (Fig. S9 [10]). While it is possible for the trapping rate to be a function of applied bias [16], here we assume it is constant, as we are primarily interested in maximized photon recycling (where charge trapping has minimal effect). Our results show that, for fixed absorptance, reducing charge trapping increases N_{mpp} and efficiency.

We next consider nonideal front transmission and back reflection, both of which can also correspond to parasitic absorption. N_{mpp} varies from 0.2 to 1 for front transmission coefficients larger than 5% [Fig. 2(c)] but reduces at higher efficiencies ($N_{mpp} < 0.3$ when efficiency

$>26.5\%$, Fig. S10 [10]). N_{mpp} is more strongly affected by front transmission than rear reflection as reducing front transmission lowers the excitation density, reducing the effects of nonradiative Auger recombination. Importantly, N_{mpp} reduces as front transmission (and consequently efficiency) is improved.

We consider the effect of light management (necessary for any optimized solar cell) on photon recycling by considering three absorptance models (Supplemental Material [10], Table 1 and Fig. S12). These represent a flat surface, a roughened surface, and an idealized surface whereby the film absorbs the maximum light possible for a given thickness, termed direct, randomized, and maximal, respectively. We consider a 500-nm thick MAPbI₃ solar cell for our three different absorptances and vary the charge trapping rate. In Fig. 3(a) we plot N_{mpp} versus efficiency, both as a function of the first-order trapping rate, for all absorptances. Randomized and maximal absorptances give higher efficiencies than direct for the same trapping rates as they lead to more light absorption. Importantly, models

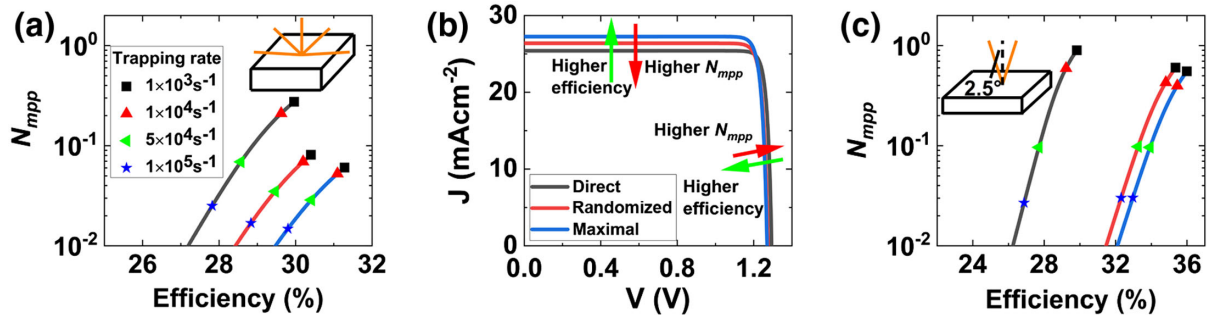


FIG. 3. (a) Relationship between the number of photon recycling events at maximum power point, N_{mpp} , and efficiency (for interaction with a full 2π hemisphere, see schematic) for MAPbI₃ solar cells in which the charge trapping rate (selected values defined in legend) is varied for different absorptance models [legend in (b)] in a 500-nm thick film. (b) Current-voltage (J-V) characteristics for the three absorptance models considered, with no charge trapping. (c) Results equivalent to (a) for a MAPbI₃ solar cell which only interacts with 2.5° of direct and circumsolar radiation (see schematic).

that yield higher efficiency also give lower N_{mpp} , due to increased escape probabilities. For example, with a loss rate of 10^5 s^{-1} , direct gives an efficiency of 27.8% and $N_{\text{mpp}} = 0.025$, while maximal yields an efficiency of 29.8% and $N_{\text{mpp}} = 0.015$. Randomized and maximal models yield a decrease in open circuit voltage (due to more reemitted light), which is more than compensated for by an increase in the short circuit current. This is demonstrated in the current-voltage (J-V) curves shown in Fig. 3(b) (see further discussion in Supplemental Material [10], Note 4). We note that the interplay between charge trapping and absorptance (treated independently here) should be considered when experimentally optimizing solar cells.

A second approach to controlling absorptance is reducing the solid angle of interaction with the surroundings, reducing reemitted light [17–19]. Therefore, we consider a solar cell which only interacts with direct and circumsolar light and present corresponding results for the three absorptance models in Fig. 3(c) using reciprocity to calculate absorptance and emittance. We note circumsolar and direct AM1.5 contains less blue light, slightly reducing

short circuit current (Fig. S13 [10]). Therefore, for direct absorptance we see a slight decrease in the maximum efficiency (from 30.0% to 29.9%), and $N_{\text{mpp}} = 0.94$ with no charge trapping. Randomized and maximal absorptance models again give higher efficiencies (maxima of 35.4% and 36.1%) and lower N_{mpp} (0.62 and 0.57). In all cases N_{mpp} is higher than in a solar cell, which interacts with a full 2π hemisphere, indicating photon recycling is more significant here. These calculations corroborate that increasing roughness reduces N_{mpp} yet improves efficiency.

We now consider CsPbBr₃ LEDs. We use a reciprocal model to our description of solar cells (see Supplemental Material [10], Note 5). We present results using the direct absorptance (here, emittance) model for a LED which emits over a full 2π hemisphere unless otherwise stated; we see similar results from other models (Figs. S14–S17 [10]). We present the number of photon recycling events in the LED, N , as a function of thickness, with no charge trapping, in Fig. 4(a). We consider an applied voltage (quasi-Fermi-level difference) that gives a luminous emittance of 1000 lm m^{-2} at 100-nm film thickness. Our calculations demonstrate photon recycling occurs significantly more

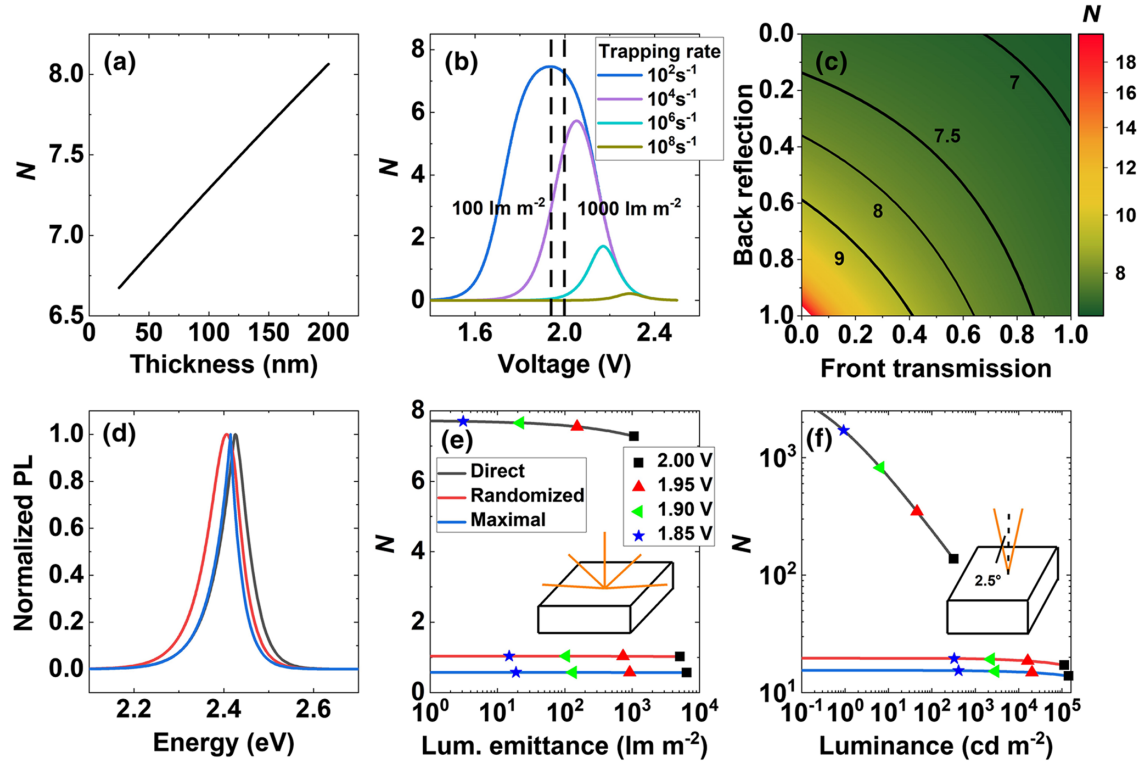


FIG. 4. Number of photon recycling events N in a CsPbBr₃ LED as a function of (a) thickness for an applied voltage that gives 1000 lm m^{-2} at 100-nm thickness (and no charge trapping), and (b) voltage for different charge trapping rates. Voltages corresponding to $100 (1.94 \text{ V})$ and $1000 \text{ lm m}^{-2} (2.00 \text{ V})$ are marked with dashed lines. (c) N (on a logarithmic scale) as a function of front transmission and back reflection coefficients. (d) Normalized photoluminescence spectra for the three emittance models. Legends in (e) apply to (d), (e) and (f). (e) N and luminous emittance as a function of applied voltage for the three emittance models, with specific voltages marked, for emission into a full 2π hemisphere (see schematic). (f) The equivalent plot to (e) for a LED that emits into a 2.5° cone about the normal to its surface (see schematic). Calculations in (b)–(f) are performed on a 100-nm thick film.

within LEDs than solar cells under operating conditions: N can be as high as 8 here. In analogy to efficiency in a solar cell (cf. Fig. S3), luminous emittance also increases with thickness (Fig. S15 [10]).

We plot N as a function of applied voltage for different first order trapping rates in a 100-nm emitter film in Fig. 4(b). Our results demonstrate that for photon recycling to be important (i.e., $N > 0.1$ at 1000 lm m^{-2}) charge trapping rates need to be $< 10^6 \text{ s}^{-1}$. Furthermore, Auger recombination reduces N at larger charge densities.

We plot N as a function of front transmission and back reflection coefficients in Fig. 4(c) (for a 100-nm thick film with no charge trapping and voltage set to give maximum forward luminous emittance of 1000 lm m^{-2}). N is equally impacted by the front and rear transmission coefficients as our model is fully symmetric. N varies relatively slowly until front transmission is less than 0.4 and back reflection greater than 0.6. Here N becomes greater than 9 and rapidly increase further for weaker front transmission. We find that forward luminous emittance is maximized for maximum front transmission and minimal back transmission (Fig. S18 [10]), unlike N .

We now consider the effects of surface roughness with our three emittance models: direct, randomized, and maximal. We note these models give slightly different photoluminescence emission spectra [Fig. 4(d)]. We plot N versus luminous emittance (both as a function of voltage) for LEDs that emit into a 2π hemisphere in Fig. 4(e). N is dramatically reduced from greater than 7 for direct to less than 1 for maximal emittance. However, maximal has the highest luminous emittance of $\sim 6000 \text{ lm m}^{-2}$, compared to $\sim 1000 \text{ lm m}^{-2}$ for the direct case at the same applied voltage, noting nonradiative Auger recombination reduces luminescence further in the latter case due to increased photon trapping. We find that rough surfaces emit more light and reduce N , as was the case for solar cells.

The difference for the three emittance models is even more evident for an LED that only emits 2.5° about the normal to the LED's surface [Fig. 4(f)], which can be achieved by use of nanostructures [20–23]. For an applied voltage giving a luminance of 100 cd m^{-2} for the direct model, $44,000 \text{ cd m}^{-2}$ is achieved with the maximal emittance model. However, as in the case of solar cells, photon recycling becomes an integral part of all optimized LEDs that only emit into a small solid angle, with $N > 10$ in all models. These collective results highlight the reciprocal nature of our model for both light absorption and light emission, and that maximum efficiency (or emitted light) is not necessarily achieved with maximum photon recycling.

In conclusion, we present a general framework to quantify the number of photon recycling events N . We apply our model to MAPbI₃ solar cells and CsPbBr₃ LEDs, revealing that even for a highly luminescent (i.e., well passivated) solar cell N is less than 1 per absorbed solar photon at maximum power point. Conversely, in LEDs N

can be as high as 8 at typical LED operating voltages, or even higher for solid angles of emission smaller than 2π . We show that photon recycling, solar cell efficiency and luminous emittance all increase for thicker cells, cells with reduced charge trapping, and cells with better back reflectors. However, better light management and front transmission for a given thickness increase efficiency and luminosity but decrease N . Our results demonstrate that absorptance and emittance should be maximized when optimizing solar cells and LEDs, even if this reduces the number of photon recycling events.

The data underlying this Letter are available at Ref. [24].

A. R. B. acknowledges funding from a Winton Studentship, Oppenheimer Studentship, and the Engineering and Physical Sciences Research Council (EPSRC) Doctoral Training Centre in Photovoltaics (CDT-PV). S. D. S. and M. A. acknowledge funding from the European Research Council (ERC) (HYPERION, Grant Agreement No. 756962) and the Marie Skłodowska-Curie actions (Grant Agreement No. 841386) under the European Union's Horizon 2020 research and innovation programme. S. D. S. acknowledges the Royal Society and Tata Group (UF150033). We thank Luis Pazos-Outón for supplying data for MAPbI₃ solar cells. This work was supported by EPSRC Grant Nos. EP/S030638/1 and EP/R023980/1. S. D. S. is a co-founder of Swift Solar Inc.

*Corresponding author.
sds65@cam.ac.uk

- [1] O. Von Roos, Influence of radiative recombination on the minority-carrier transport in direct band-gap semiconductors, *J. Appl. Phys.* **54**, 1390 (1983).
- [2] J. E. Parrott, Radiative recombination and photon recycling in photovoltaic solar cells, *Sol. Energy Mater. Sol. Cells* **30**, 221 (1993).
- [3] L. M. Pazos-Outon, M. Szumilo, R. Lamboll, J. M. Richter, M. Crespo-Quesada, M. Abdi-Jalebi, H. J. Beeson, M. Vrućinić, M. Alsari, H. J. Snaith, B. Ehrler, R. H. Friend, and F. Deschler, Photon recycling in lead iodide perovskite solar cells, *Science* **351**, 1430 (2016).
- [4] C. Cho, B. Zhao, G. D. Tainter, J. Y. Lee, R. H. Friend, D. Di, F. Deschler, and N. C. Greenham, The role of photon recycling in perovskite light-emitting diodes, *Nat. Commun.* **11**, 611 (2020).
- [5] J. Nelson, *The Physics of Solar Cells* (Imperial College Press, London, 2003).
- [6] U. Rau, U. W. Paetzold, and T. Kirchartz, Thermodynamics of light management in photovoltaic devices, *Phys. Rev. B* **035211**, 1 (2014).
- [7] T. W. Crothers, R. L. Milot, J. B. Patel, E. S. Parrott, J. Schlipf, P. Müller-Buschbaum, M. B. Johnston, and L. M. Herz, Photon reabsorption masks intrinsic bimolecular charge-carrier recombination in CH₃NH₃PbI₃ perovskite, *Nano Lett.* **17**, 5782 (2017).

- [8] T. Kirchartz, F. Staub, and U. Rau, Impact of photon recycling on the open-circuit voltage of metal halide perovskite solar cells, *ACS Energy Lett.* **1**, 731 (2016).
- [9] R. Brenes, M. Laitz, J. Jean, D. W. Dequillettes, and V. Bulović, Benefit from Photon Recycling at the Maximum-Power Point of State-of-the-Art Perovskite Solar Cells, *Phys. Rev. Applied* **12**, 014017 (2019).
- [10] See Supplemental Material at <http://link.aps.org/supplemental/10.1103/PhysRevLett.125.067401> for discussion of data and models used, and additional simulation results to support the results shown in the main text.
- [11] W. van Roosbroeck and W. Shockley, Photon-radiative recombination of electrons and holes in germanium, *Phys. Rev.* **94**, 1558 (1954).
- [12] J. C. De Mello, H. F. Wittmann, and R. H. Friend, An improved experimental determination of external photoluminescence quantum efficiency, *Adv. Mater.* **9**, 230 (1997).
- [13] S. D. Stranks, G. E. Eperon, G. Grancini, C. Menelaou, M. J. P. Alcocer, T. Leijtens, L. M. Herz, A. Petrozza, and H. J. Snaith, Electron-hole diffusion lengths exceeding 1 micrometer in an organometal trihalide perovskite absorber, *Science* **342**, 341 (2013).
- [14] L. M. Pazos-Outón, T. P. Xiao, and E. Yablonovitch, Fundamental efficiency limit of lead iodide perovskite solar cells, *J. Phys. Chem. Lett.* **9**, 1703 (2018).
- [15] D. W. DeQuillettes, S. Koch, S. Burke, R. K. Paranj, A. J. Shropshire, M. E. Ziffer, and D. S. Ginger, Photoluminescence lifetimes exceeding $8\ \mu\text{s}$ and quantum yields exceeding 30% in hybrid perovskite thin films by ligand passivation, *ACS Energy Lett.* **1**, 438 (2016).
- [16] M. V. Khenkin, K. M. Anoop, E. A. Katz, and I. Visoly-Fisher, Bias-dependent degradation of various solar cells: Lessons for stability of perovskite photovoltaics, *Energy Environ. Sci.* **12**, 550 (2019).
- [17] O. Höhn, T. Kraus, G. Bauhuis, U. T. Schwarz, and B. Bläsi, Maximal power output by solar cells with angular confinement, *Opt. Express* **22**, A715 (2014).
- [18] M. Peters, C. Ulbrich, J. C. Goldschmidt, J. Fernandez, G. Siefer, and B. Bläsi, Directionally selective light trapping in a germanium solar cell, *Opt. Express* **19**, A136 (2011).
- [19] C. Ulbrich, M. Peters, B. Bläsi, T. Kirchartz, A. Gerber, and U. Rau, Enhanced light trapping in thin-film solar cells by a directionally selective filter, *Opt. Express* **18**, A133 (2010).
- [20] G. Lozano, G. Grzela, M. A. Verschuuren, M. Ramezani, and J. G. Rivas, Tailor-made directional emission in nano-imprinted plasmonic-based light-emitting devices, *Nano-scale* **6**, 9223 (2014).
- [21] S. Zhang, G. A. Turnbull, and I. D. W. Samuel, Highly directional emission and beam steering from organic light-emitting diodes with a substrate diffractive optical element, *Adv. Opt. Mater.* **2**, 343 (2014).
- [22] S. H. Yang, T. J. Huang, and T. H. Liu, High color rendering index and directional emission of white OLEDs using nanorod waveguide channels, *J. Lumin.* **201**, 402 (2018).
- [23] J. Dimaria, E. Dimakis, T. D. Moustakas, and R. Paiella, Plasmonic off-axis unidirectional beaming of quantum-well luminescence, *Appl. Phys. Lett.* **103**, 1 (2013).
- [24] Alan R. Bowman, Miguel Anaya, Neil C. Greenham, and Samuel D. Stranks, [10.17863/CAM.54726](https://doi.org/10.17863/CAM.54726) (2020).